ACADEMIC PRESS

Available online at www.sciencedirect.com
SCIENCE DIRECT®

Journal of Catalysis 217 (2003) 457–467

JOURNAL OF CATALYSIS

www.elsevier.com/locate/jcat

MCM-41-supported iron phosphate catalyst for partial oxidation of methane to oxygenates with oxygen and nitrous oxide

Xiaoxing Wang, Ye Wang,* Qinghu Tang, Qian Guo, Qinghong Zhang, and Huilin Wan

State Key Laboratory for Physical Chemistry of Solid Surfaces, Department of Chemistry, Xiamen University, Xiamen 361005, China

Received 27 November 2002; revised 14 February 2003; accepted 19 February 2003

Abstract

Iron phosphate supported on MCM-41 has been studied for partial oxidation of methane with both oxygen and nitrous oxide. Characterizations with XRD, Raman spectroscopy, XPS, and H_2-TPR suggest that the supported iron phosphate species with loading amounts lower than 40 wt% are located and dispersed in the mesopores of MCM-41. Such iron phosphate species can be reduced more readily than the unsupported iron phosphate at lower temperatures. Methane is selectively converted to methanol, formaldehyde, and dimethyl ether over the supported and the unsupported iron phosphate with nitrous oxide at milder temperatures (300–500 °C), while formaldehyde is mainly produced along with carbon oxides with oxygen at relatively higher temperatures (400–600 °C). The supporting of iron phosphate onto MCM-41 with loading amounts of ca. 20–40 wt% increases both methane conversion and overall selectivity to useful oxygenates with either oxygen or nitrous oxide. Kinetic studies indicate that the activation of oxygen occurs rapidly, while the activation of nitrous oxide proceeds at a comparable rate with the conversion of methane by the active oxygen species over both the supported and the unsupported catalysts. The supported catalyst, however, enhances the activation of nitrous oxide and thus remarkably inhibits the carbon deposition occurring over the unsupported iron phosphate.

Keywords: Iron phosphate; MCM-41; Methane partial oxidation; Oxygenates; Nitrous oxide

1. Introduction

Partial oxidation of methane directly to useful oxygenates such as methanol and formaldehyde remains as a great challenge in the new century. Although a large number of catalysts and several novel processes have been reported, none of them has satisfied the requirements for commercialization [1–7].

One of the present authors has found that an iron phosphate ($FePO_4$) catalyst shows high selectivity to useful oxygenates including CH_3OH and HCHO during the partial oxidation of CH_4 with H_2–O_2 gas mixtures or N_2O under milder reaction temperatures (< 500 °C) [8–11]. $FePO_4$ was also a good catalyst for the formation of HCHO with O_2 alone, although the oxidation of CH_4 proceeded at relatively higher temperatures [8]. It has been clarified that the tetrahedrally coordinated iron site surrounded by phosphate groups plays important roles in the selective oxidation of CH_4 [12]. The reports by other two groups [13,14] also confirmed the importance of the coordination environments of iron in Fe-containing silica catalysts for partial oxidation of CH_4.

Although $FePO_4$ showed high selectivity to useful oxygenates in partial oxidation of CH_4 particularly with N_2O, the conversion of CH_4 was still to be increased. Recently, McCormick and co-workers [15,16] found that the supporting of $FePO_4$ onto silica enhanced the conversion of CH_4 to HCHO with O_2. Since MCM-41, one of the mesoporous molecular sieves, possesses well-ordered mesoporous channels with controllable pore sizes from 2 to 10 nm and large surface areas, the active component may thus be tailored in the nano-order space of MCM-41. Many metal ion or metal oxide-containing MCM-41 materials have been used as selective oxidation catalysts [17–21]. Vanadium oxide supported on MCM-41 prepared by an impregnation method was reported to exhibit high activity for the partial oxidation of CH_4 to HCHO with O_2 [18]. In the present paper, we report the structural and catalytic properties of the $FePO_4$ supported on MCM-41 for partial oxidation of CH_4 with both O_2 and N_2O. The catalytic properties and kinetic fea-

* Corresponding author.
E-mail address: yewang@jingxian.xmu.edu.cn (Y. Wang).

0021-9517/03/$ – see front matter
doi:10.1016/S0021-9517(03)00077-0

tures of the supported catalysts are compared with those of the unsupported $FePO_4$ to elucidate the supporting effects and gain insight into the reaction mechanism.

2. Experimental

2.1. Catalyst

$FePO_4$ was prepared using the procedure described previously [8]. The aqueous solutions of $Fe(NO_3)_3$ and $NH_4H_2PO_4$ were mixed followed by evaporation at 70 °C with continuous stirring. The resultant was calcined at 550 °C for 6 h.

MCM-41 was prepared by hydrothermal synthesis at 120 °C for 96 h using sodium silicate, and hexadecyltrimethylammonium bromide as the sources of silicon and template, respectively. The details of the procedures were described in our previous papers [19,21]. After hydrothermal synthesis, the resultant solid was washed with deionized water, dried at 40 °C in vacuum, and finally calcined at 550 °C for 6 h.

MCM-41 supported $FePO_4$ catalysts were prepared by an impregnation method. A certain amount of MCM-41 was immersed into the mixed aqueous solution of $Fe(NO_3)_3$ and $NH_4H_2PO_4$ ($Fe/P = 1$) and was allowed to stir for ca. 12 h at room temperature. The slurry was then dried at 70 °C with continuous stirring. The dried powder was finally calcined at 550 °C for 6 h.

2.2. Characterization

X-ray diffraction (XRD) measurements were performed with a Rigaku D/Max-C X-ray diffractometer with Cu-K_α radiation (40 kV, 40 mA). For determining the mesoporous regularity of MCM-41, small divergent and scattering slits (0.05 mm) were selected to avoid a high background at low diffraction angles ($2\theta = 1$–$8°$).

N_2 adsorption at 77 K was carried out with a TriStar 3000 surface area and porosimetry analyzer (Micromeritics) to examine the porous property and the surface area of each sample. All the samples were pretreated at 300 °C for 3 h before N_2 adsorption. The pore diameter distribution was evaluated from the adsorption isotherm by the BJH method.

Raman spectroscopic measurements were carried out with a Renishaw UV–Vis Raman System 1000R. The UV line at 325 nm from a Kimmon IK3201R-F He-Cd laser was used as the exciting source to avoid the influence of serious fluorescence. A laser output of 30 mW was used and the maximum incident power at the sample was approximately 6 mW in each measurement.

X-ray photoelectron spectroscopy (XPS) was measured with a Quantum 2000 Scanning ESCA Microprob equipment (Physical Electronics) using Al-K_α radiation. The binding energy was calibrated using a C1s photoelectron peak at 284.6 eV as a reference. The surface composition was determined from the peak areas and the sensitive factors presented by Physical Electronics.

H_2-temperature-programmed reduction (H_2-TPR) was performed using a flow system equipped with a thermal conductivity detector. Typically, 100 mg of sample was first pretreated in a quartz reactor with a gas flow containing O_2 and N_2 at 550 °C for 1 h followed by purge with pure N_2. After cooling to 30 °C, a H_2–Ar (5% H_2) mixture was introduced into the reactor and the temperature was raised to 800 °C at a rate of 10 °C min^{-1}.

2.3. Catalytic reaction

The catalytic reactions were carried out using a fixed-bed reactor operated at atmospheric pressure. The catalyst was pretreated in the quartz reactor (U-type, inner diameter 4 mm) with a gas flow containing He (50 ml min^{-1}) and O_2 (10 ml min^{-1}) at 550 °C for 1 h followed by purge with He (60 ml min^{-1}) at the same temperature for 1 h before reaction. The reaction was started by introducing the gas flow of mixed He, CH_4, and O_2 or N_2O to the reactor. The products were analyzed by two on-line gas chromatographs. All the lines and valves between the exit of the reactor and the gas chromatographs were heated to 120 °C to prevent the condensation of the products. A TSR-1 (10%/Flusin T) column was used for the separation of CH_3OH, HCHO, and H_2O in our previous studies [8–11], but recently, we found that CH_3OCH_3 could not be separated with HCHO on the same column. Thus, CH_3OCH_3 was not appropriately quantified in our previous work. The separation of CH_3OH, HCHO, CH_3OCH_3, and H_2O was easily achieved with a Porapak T column in this work, and the formation of CH_3OCH_3 was confirmed by GC-MS. The separations of other components such as O_2, CH_4, CO, and CO_2 were carried out on two other columns, Porapak Q and Molecular Sieve 5 A. The results after 1 h of reaction were typically shown and used for discussion, unless otherwise stated.

The conversion of CH_4 and the selectivities to partial oxidation products were evaluated on the basis of the amount (mol) of all the carbon-containing products formed and that of the CH_4 remaining in the effluent. In other words, CH_4 conversion and product selectivity were calculated using the following equations,

$$\begin{aligned}&\text{CH}_4\text{ conversion}\\&= \big[\big([\text{CH}_3\text{OH}] + [\text{HCHO}] + 2[\text{CH}_3\text{OCH}_3]\\&\quad + [\text{CO}] + [\text{CO}_2]\big)\big/\big([\text{CH}_4] + [\text{CH}_3\text{OH}] + [\text{HCHO}]\\&\quad + 2[\text{CH}_3\text{OCH}_3] + [\text{CO}] + [\text{CO}_2]\big)\big] \times 100\%\end{aligned}$$

$$\begin{aligned}&\text{product selectivity}\\&= \big[n[\text{product}]\big/\big([\text{CH}_3\text{OH}] + [\text{HCHO}] + 2[\text{CH}_3\text{OCH}_3]\\&\quad + [\text{CO}] + [\text{CO}_2]\big)\big] \times 100\%,\end{aligned}$$

where $n = 1$ for CH_3OH, HCHO, CO, and CO_2 and $n = 2$ for CH_3OCH_3.

The relative error estimated for CH_4 conversion and product selectivity was within ±5%. Carbon balance was also checked in some cases, and the values were better than 95%.

3. Results and discussion

3.1. Structural properties of supported iron phosphate

Table 1 shows the porous properties of MCM-41-supported $FePO_4$ catalysts determined from N_2-adsorption measurements at 77 K. The BET surface area and pore volume were decreased with increasing loading amount of $FePO_4$ up to ca. 40 wt%. Further increase in the loading amount from 40 to 60 wt% did not significantly affect either the surface area or the pore volume. The pore diameter distribution evaluated by the BJH method is shown in Fig. 1. The pore diameter changed in a manner similar to that for surface area and pore volume, decreasing as the loading amount of $FePO_4$ increased up to ca. 40 wt% and keeping almost unchanged with a further increase in the loading amount. Such a tendency probably suggests that the $FePO_4$ with a maximum loading amount of ca. 40 wt% may be incorporated into the mesopores of MCM-41. It should be noted that $FePO_4$ itself exhibited a very low surface area of 3.0 m^2/g.

Table 1
Porous properties of MCM-41-supported $FePO_4$ with different loading amount

Sample	Surface area ($m^2\ g^{-1}$)	Pore volume ($cm^3\ g^{-1}$)	Pore diameter (nm)
MCM-41	905	0.82	3.2
9 wt% $FePO_4$/MCM-41	689	0.56	3.0
20 wt% $FePO_4$/MCM-41	556	0.46	2.9
40 wt% $FePO_4$/MCM-41	310	0.19	2.7
60 wt% $FePO_4$/MCM-41	304	0.25	2.8
$FePO_4$	3.0	–	–

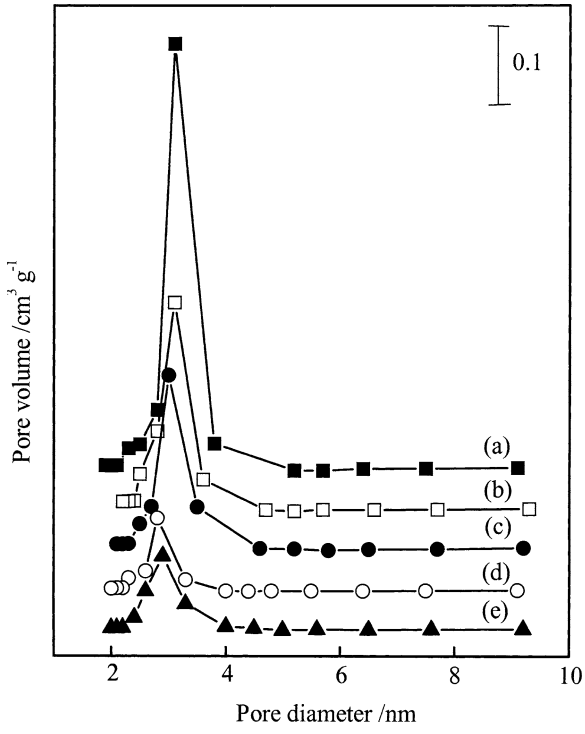

Fig. 1. Pore diameter distributions. (a) MCM-41, (b) 9 wt% $FePO_4$/MCM-41, (c) 20 wt% $FePO_4$/MCM-41, (d) 40 wt% $FePO_4$/MCM-41, (e) 60 wt% $FePO_4$/MCM-41.

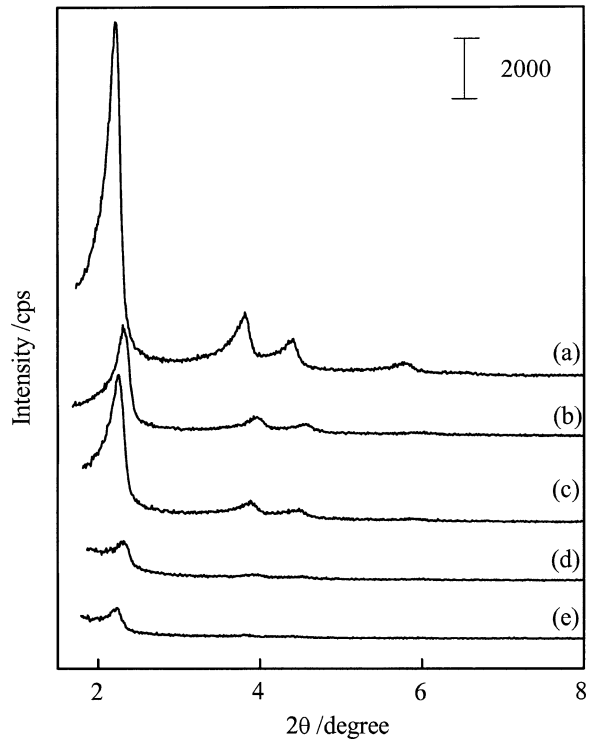

Fig. 2. XRD patterns at low diffraction angles. (a) MCM-41, (b) 9 wt% $FePO_4$/MCM-41, (c) 20 wt% $FePO_4$/MCM-41, (d) 40 wt% $FePO_4$/MCM-41, (e) 60 wt% $FePO_4$/MCM-41.

XRD results at low diffraction angles ($2\theta = 1$–$8°$) in Fig. 2 show that MCM-41 exhibits four diffraction lines indexed to its typical hexagonal regularity of mesoporous channel. The supporting of $FePO_4$ onto MCM-41 decreased the intensity of these lines. The decrease became much notable when the loading amount reached 40 wt%, but the hexagonal regularity was still observable even for the sample with 40 wt% of $FePO_4$. The decrease in peak intensity indicated the deorganization at long range of the mesoporous structure. Although the collapse of mesopores could be a reason, we think that the incorporation of $FePO_4$ species into the mesopores may also result in the irregularity at long range and thus cause the drop in the intensity of XRD peaks. No definite tendency in the shift of peak position was observed with changing the loading amount of $FePO_4$ as shown in Fig. 2. We speculate that this may arise from the fact that the wall of MCM-41 is amorphous and not very rigid, and thus the wall thickness may be slightly varied during the impregnation process.

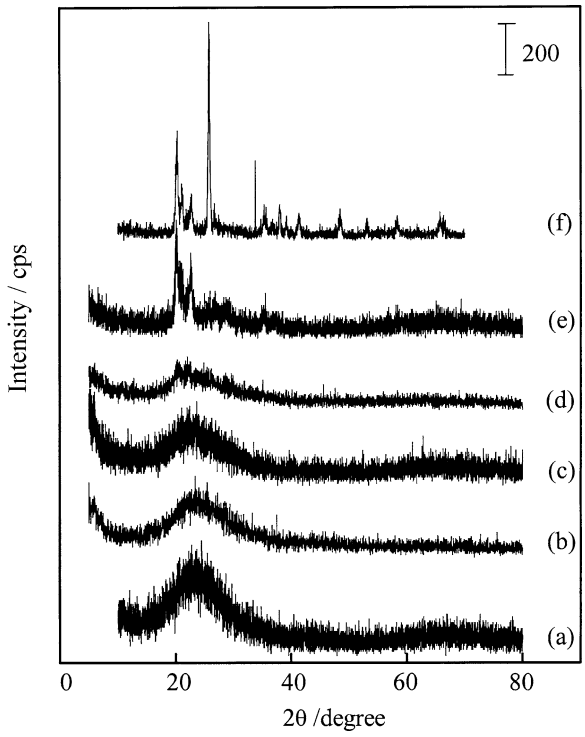

Fig. 3. XRD patterns at high diffraction angles. (a) MCM-41, (b) 9 wt% $FePO_4$/MCM-41, (c) 20 wt% $FePO_4$/MCM-41, (d) 40 wt% $FePO_4$/MCM-41, (e) 60 wt% $FePO_4$/MCM-41, (f) $FePO_4$.

XRD patterns at high diffraction angles ($2\theta = 10$–$80°$) are shown in Fig. 3. The unsupported $FePO_4$ (curve f) was composed of mainly a quartz-like phase as well as a small amount of a tridymite-like phase (three lines at $2\theta = 20.2$, 21.1, and 22.7° are assigned to the tridymite-like phase, but that at $2\theta = 20.2°$ can also be from the (100) index of the quartz-like phase). Recently, using in situ XRD/EXAFS, Beale and Sankar [22] revealed that the tridymite-like phase was firstly formed from ca. 100 °C during the heating of the precursor of $FePO_4$ prepared by a hydrothermal synthesis method, and the tridymite-like phase was transformed to the quartz-like phase above ca. 500 °C. We have also checked the change of XRD pattern of $FePO_4$ with the calcination temperature in our case. After calcination at 450 °C, the strongest line of the quartz-like phase ($2\theta = 25.8°$) did not appear and only weak diffraction lines at $2\theta = 20.5$ and 22.5° assignable to the tridymite-like phase (the former one can also be assigned to the (100) index of the quartz-like phase) were observed. Most peaks of the quartz-like phase became observable after the calcination at 550 °C, and the intensity of these peaks increased remarkably with the calcination temperature.

As shown in Fig. 3, for the MCM-41-supported $FePO_4$ samples, any crystalline phase of $FePO_4$ did not appear when the loading amount was lower than 40 wt%. Two weak lines at 20.5 and 22.0° assignable to the tridymite-like phase (the former one can also be assigned to the (100) index of the quartz-like phase) became observable for the sample with a loading amount of 40 wt% (curve d). The intensity of diffraction lines increased largely and three peaks at 20.2, 21.2, and 22.5° appeared as the loading amount rose to 60 wt% (curve e). However, the strongest line of the quartz-like phase at 25.8° was still not observed, although all these supported samples were calcined at 550 °C. It is interesting to note that McCormick and co-workers [15] found the easy formation of the quartz-like phase of $FePO_4$ on a silica support even with only 5 wt% loading. These results allow us to consider that most of the $FePO_4$ species with loading amounts of lower than 40 wt% are probably located inside the mesopores, dispersing on the wall surface of MCM-41 or forming small clusters which are hard to be detected by XRD. As the loading amount arrived at or exceeded 40 wt%, the clusters began to aggregate outside the mesopores to form a small crystalline tridymite-like $FePO_4$ phase or a mixed phase containing both the tridymite-like $FePO_4$ and the quartz-like one with its (100) face predominantly exposed.

Fig. 4 shows the Raman spectra of the supported and the unsupported $FePO_4$. $FePO_4$ exhibited two intense Raman bands at 1017 and 1075 cm^{-1} along with weak bands at 400–700 and 1182 cm^{-1}. It is generally accepted that the stretching and bending vibrations of phosphate groups occur at 1000–1200 and 400–700 cm^{-1}, respectively [23]. However, we recently found that the tetrahedrally coordinated iron in the framework of ferrisilicate with an MFI structure and MCM-41 also exhibited Raman bands at 1000–1200 and 400–700 cm^{-1} if the UV laser of 325 nm was used as the exciting source. With a visible laser of 514 nm as the ex-

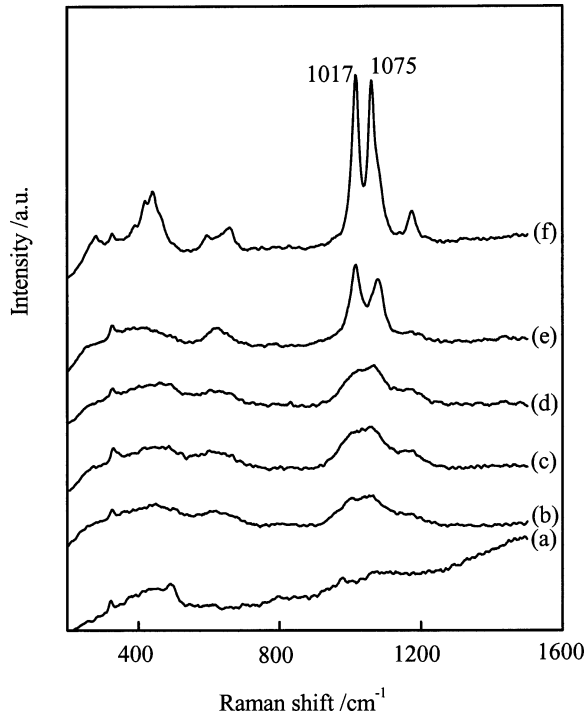

Fig. 4. Laser Raman spectra. (a) MCM-41, (b) 9 wt% $FePO_4$/MCM-41, (c) 20 wt% $FePO_4$/MCM-41, (d) 40 wt% $FePO_4$/MCM-41, (e) 60 wt% $FePO_4$/MCM-41, (f) $FePO_4$.

citing source, almost no Raman band was observed for the ferrisilicate or Fe-MCM-41, but a band at 1014 cm^{-1} appeared distinctly for $FePO_4$. Thus, we tentatively suggest that the intense bands at 1017 and 1075 cm^{-1} observed for $FePO_4$ with the UV laser as the exciting source might arise from the phosphate groups and the tetrahedrally coordinated iron sites, respectively. The latter one was enhanced by using UV laser as the exciting source and may thus be the UV resonance Raman band. The two bands were still observable for the MCM-41-supported $FePO_4$ samples, but they became broad and overlapped. It is noticeable that the two bands became sharp and well separated when the loading amount of $FePO_4$ increased to 60 wt%. These results suggest that the local structure for the $FePO_4$ species dispersed inside the mesopores of MCM-41 is probably similar to that for the bulk $FePO_4$, although the former do not have regularity at long ranges. The broadening of the Raman peaks may be related to the high dispersion or the small size of the $FePO_4$ species inside the mesopores.

Fig. 5 shows the Fe 2p, P 2p, and O 1s XPS spectra for the unsupported and supported $FePO_4$ samples. The binding energies of Fe 2p3/2, P 2p, O 1s, and Si 2p and the atomic ratios of Fe/P and Fe/Si of each sample are summarized in Table 2. The binding energy of P 2p for the samples with loading amounts of 9 and 40 wt% shifted to higher a position as compared with that for the unsupported $FePO_4$. The binding energy of Fe 2p3/2 for the sample with a loading amount of 9 wt% was relatively lower as shown in Table 2. However, the ratio of signal to noise in this case was too low to give a precise value of peak position. The reason for the shift in the binding energy of P 2p is not clear at this moment. The binding energy of O 1s for all the supported samples was remarkably larger than that for the unsupported one, and was almost the same as that for MCM-41. It can be seen from Fig. 5 that the O 1s spectra for the samples with loading amounts of 40 and 60 wt% are slightly asymmetric and can be separated into two components (dashed line), i.e., one smaller component with the maximum similar to that for the unsupported $FePO_4$ and one larger component with the peak resembling that for the support. The lower Fe/P ratio observed for the unsupported $FePO_4$ indicated the surface enrichment in phosphorus. The Fe/P ratios examined by XPS for the supported samples became higher and closer to 1.0, suggesting that the loading of $FePO_4$ to MCM-41 could reduce the surface enrichment in phosphorus. The values of the Fe/Si ratio for the supported samples were remarkably lower than those expected from the calculation based on the loading amount, e.g., 0.029 observed from XPS versus 0.26 as expected for the 40 wt% $FePO_4$/MCM-41. Such a large discrepancy and the similarity of O 1s binding energy of the supported samples to that of MCM-41 may further support that most of the $FePO_4$ species are incorporated inside the mesopores of MCM-41.

Fig. 6 shows H_2-TPR profiles for the MCM-41 supported and the unsupported $FePO_4$. The unsupported $FePO_4$ exhibited one asymmetric reduction peak with the maximum

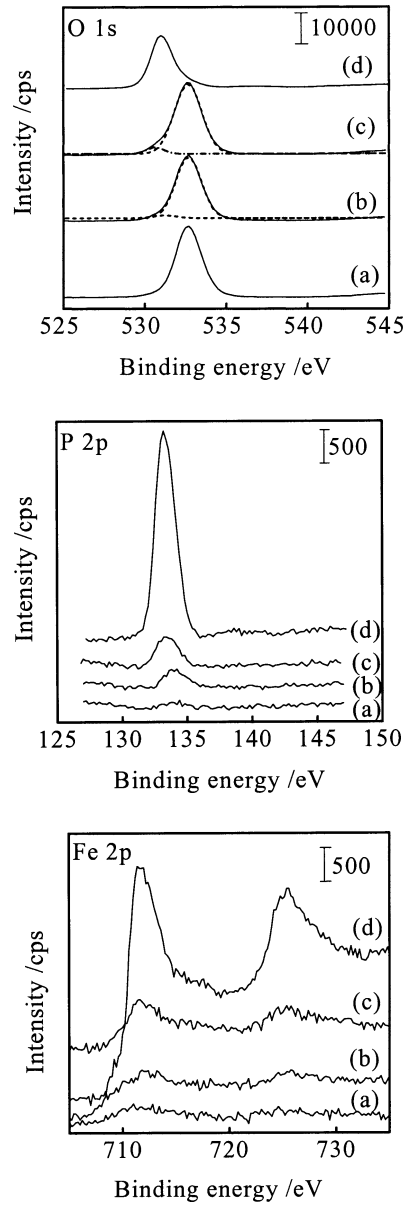

Fig. 5. XPS spectra of Fe 2p, P 2p, and O 1s. (a) 9 wt% $FePO_4$/MCM-41, (b) 40 wt% $FePO_4$/MCM-41, (c) 60 wt% $FePO_4$/MCM-41, (d) $FePO_4$. The dashed lines represent the peak separation results.

at 672 °C. It should be noted that almost the same peak position was observed when a smaller amount (20 mg) of the unsupported $FePO_4$ sample was used in the same experiment. This suggests that the peak position cannot be shifted significantly only by varying the amount of reducible species in our case. The quantification indicated that this peak corresponded to almost the complete reduction of the bulk $FePO_4$ to $Fe_2P_2O_7$. Since the $FePO_4$ used here consists of a small proportion of a tridymite-like phase in addition to the main quartz-like phase as indicated in Fig. 3, we speculate that the asymmetric peak may result from the reduction of the tridymite-like phase at the first stage and then the reduction of the quartz-like phase at the second stage. Actually, the shift of peak temperature from 645 to

Table 2
XPS results obtained for the MCM-41-supported iron phosphate catalysts

Sample	Binding energy (eV)				Fe/P atomic ratio	Fe/Si atomic ratio
	Fe 2p 3/2	P 2p	O 1s	Si 2p		
MCM-41	–	–	532.5	103.5	–	–
9 wt% $FePO_4$/MCM-41	710.5	133.9	532.5	103.3	1.16	0.016
40 wt% $FePO_4$/MCM-41	711.4	133.8	532.6	103.5	0.80	0.029
60 wt% $FePO_4$/MCM-41	711.3	133.1	532.5	103.3	0.81	0.050
$FePO_4$	711.4	133.1	530.9	–	0.59	–

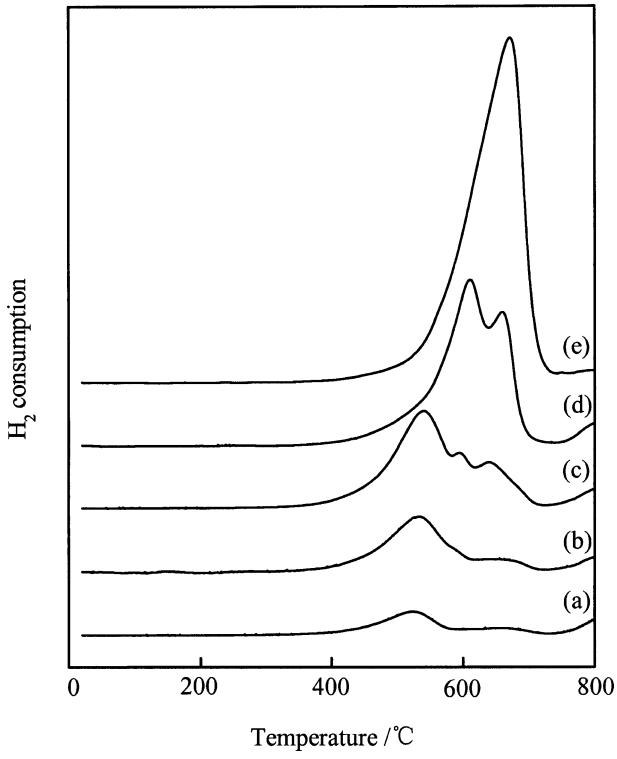

Fig. 6. H_2-TPR profiles. (a) 9 wt% $FePO_4$/MCM-41, (b) 20 wt% $FePO_4$/MCM-41, (c) 40 wt% $FePO_4$/MCM-41, (d) 60 wt% $FePO_4$/MCM-41, (e) $FePO_4$.

706 °C was observed when the calcination temperature for $FePO_4$ was increased from 450 to 700 °C. This is consistent with our speculation because the tridymite-like phase was formed at relatively low temperatures and was gradually transformed to the quartz-like phase at > 500 °C as described above. It can be seen from Fig. 6 that the reduction of the $FePO_4$ species supported on MCM-41 occurs at remarkably lower temperatures as compared with the bulk $FePO_4$. The main reduction peak for the samples with loading amounts of 9–40 wt% located at 523–540 °C, and the area of this peak increased with increased loading amounts of $FePO_4$. Two shoulder peaks at 594 and 630 °C were observed for the sample with a loading amount of 40 wt%. Two peaks at 611 and 664 °C were mainly observed for the sample with a loading amount of 60 wt%. Therefore, $FePO_4$ species with different structures or locations exhibited different redox properties. Combining with the XRD patterns shown in Fig. 3, the results obtained here strongly suggest that the highly dispersed $FePO_4$ species, which cannot be detected by XRD and are possibly located inside the mesopores of MCM-41, are reduced at the lowest temperature. The reduction of such species could start from temperatures of ca. 400 °C and arrive at a maximum at 520–540 °C. On the other hand, the reduction with maxima at ca. 600 °C and temperatures higher than 650 °C may arise from the reduction of the crystalline $FePO_4$ phases, i.e., the tridymite-like and the quartz-like phases, respectively.

3.2. Catalytic properties of supported iron phosphates in the partial oxidation of methane with oxygen

To make good comparisons between the unsupported and the supported catalysts, we fixed catalyst weight ($W = 0.5$ g for $FePO_4$ and 0.2 g for the supported samples), total flow rate ($F = 60$ ml min^{-1}), and partial pressures of reactants ($P(CH_4) = 33.8$ kPa, $P(O_2) = 16.9$ kPa, or $P(N_2O) = 33.8$ kPa) in most of our experiments. The temperature regions investigated were 400–600 and 300–500 °C in the cases of using O_2 and N_2O, respectively. These conditions could give reasonably good selectivities to partial oxidation products, and no reaction occurred without catalyst under these conditions.

Table 3 compares the catalytic properties of the supported $FePO_4$ samples with the unsupported sample in the partial oxidation of CH_4 with O_2 at 500 and 550 °C. HCHO was the only partial oxidation product in this case. MCM-41 itself also exhibited some activity for the oxidation of CH_4 with O_2, although CH_4 conversion was low. The supporting of $FePO_4$ to MCM-41 increased CH_4 conversion, and all the supported catalysts except for the one with the lowest loading amount (9 wt%) showed higher CH_4 conversion than the unsupported $FePO_4$; the conversion of CH_4 over the 40 wt% $FePO_4$/MCM-41 increased to ca. 1.7 times higher than the unsupported $FePO_4$ at 550 °C, although a lesser amount (0.2 g) of the supported catalyst was used in the reaction. More interestingly, not only the conversion of CH_4 but the selectivity to HCHO was also improved over the supported catalysts. The samples with loading amounts of 20 and 40 wt% showed remarkably higher HCHO selectivity than either the unsupported $FePO_4$ or MCM-41 at both temperatures. The space time yield of HCHO over the 40 wt% $FePO_4$/MCM-41 was 2.0 mol h^{-1} kg$_{cat}^{-1}$ under the conditions shown in Table 3 (550 °C) and could be raised to 8.9 mol h^{-1} kg$_{cat}^{-1}$ when the following conditions were used:

Table 3
MCM-41-supported iron phosphate catalysts for partial oxidation of methane using oxygen

Catalyst	T (°C)	CH_4 conversion (%)	HCHO selectivity (%)	HCHO yield (%)
MCM-41	500	0.21	42.4	0.09
	550	0.60	41.9	0.25
9 wt% $FePO_4$/MCM-41	500	0.30	58.2	0.17
	550	0.88	37.7	0.33
20 wt% $FePO_4$/MCM-41	500	0.41	79.2	0.33
	550	0.99	58.1	0.58
40 wt% $FePO_4$/MCM-41	500	0.40	79.3	0.32
	550	1.53	48.0	0.73
60 wt% $FePO_4$/MCM-41	500	0.69	66.2	0.46
	550	1.96	39.9	0.78
$FePO_4$	500	0.32	46.2	0.15
	550	0.91	39.7	0.36

Reaction conditions: $P(CH_4) = 33.8$ kPa; $P(O_2) = 16.9$ kPa; catalyst, 0.20 g for supported catalysts and 0.5 g for $FePO_4$; total flow rate, 60 ml min^{-1}.

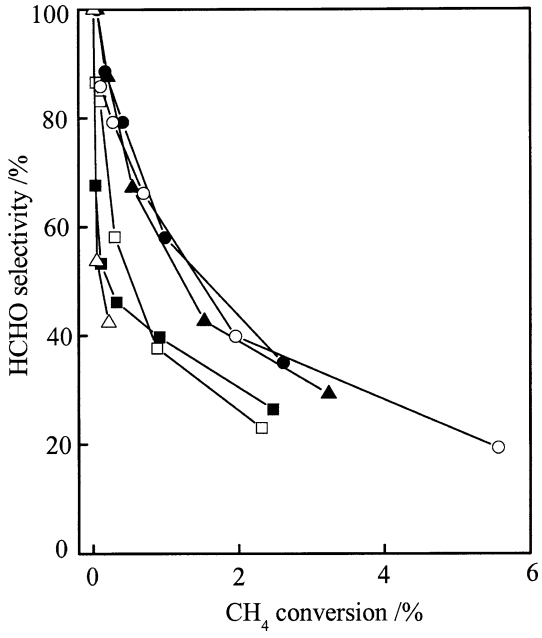

Fig. 7. HCHO selectivity versus CH_4 conversion with O_2. (△) MCM-41, (□) 9 wt% $FePO_4$/MCM-41, (●) 20 wt% $FePO_4$/MCM-41, (▲) 40 wt% $FePO_4$/MCM-41, (○) 60 wt% $FePO_4$/MCM-41, (■) $FePO_4$. Conditions: $W = 0.20$ g (for supported catalysts) and 0.50 g (for $FePO_4$), $F = 60$ ml/min, $P(CH_4) = 33.8$ kPa, $P(O_2) = 16.9$ kPa, $T = 400$–600 °C.

$W = 0.1$ g, $T = 600$ °C, $P(CH_4) = P(O_2) = 50.5$ kPa, $F = 120$ ml min^{-1}.

The selectivity to HCHO versus CH_4 conversion for the results at different temperatures (400–600 °C) is plotted in Fig. 7. All the supported catalysts exhibited higher HCHO selectivity than the unsupported $FePO_4$ and MCM-41 at the same CH_4 conversion level except for the sample with loading amounts of 9 wt%, over which HCHO selectivity decreased sharply at CH_4 conversions higher than 1%. These results suggest that the $FePO_4$ species dispersed in the mesopores of MCM-41 possess noticeable advantages over the bulk $FePO_4$ for the selective oxidation of CH_4 to HCHO with O_2.

3.3. Catalytic properties of supported iron phosphates in the partial oxidation of methane with nitrous oxide

The oxidation of CH_4 with N_2O proceeded at remarkably lower temperatures than that with O_2. Table 4 shows the catalytic results of the MCM-41-supported $FePO_4$ samples along with MCM-41 and $FePO_4$ at 400 and 450 °C. HCHO was still the only partial oxidation product over MCM-41 with N_2O. Consistent with the previous reports [9,10], CH_3OH and HCHO were produced with high selectivities over the unsupported $FePO_4$, but CH_3OCH_3 had not been appropriately quantified in those papers. As shown in Table 4, CH_3OCH_3 was formed with a selectivity of 34.5% at 400 °C over $FePO_4$. By taking into account the CH_3OCH_3 formed, the selectivity to oxygenates including CH_3OH, HCHO, and CH_3OCH_3 (selectivity to oxygenates means the sum of the selectivities to CH_3OH, HCHO, and CH_3OCH_3 hereafter) reaches 93.4% with CH_4 conversion of 0.87% at 400 °C. The selectivity to CH_3OH and CH_3OCH_3 decreased but that to HCHO increased after the supporting of $FePO_4$ to MCM-41. As compared with the unsupported $FePO_4$, the supported sample with loading amounts of 40 wt% exhibited both higher CH_4 conversion and higher selectivity to oxygenates. Since the activity of MCM-41 was very low and negligible under the conditions in Table 4, the catalytic performance of the supported catalysts was mainly due to the contribution of $FePO_4$ species. We thus also provided the rate of oxygenate formation, i.e., the sum of CH_3OH, HCHO, and CH_3OCH_3 formation rates, based on the amount of $FePO_4$ species (per gram of $FePO_4$) existing in each catalyst in Table 4. The comparison in such a way showed that the rates of oxygenate formation over the catalysts with loading amounts of 9 and 20 wt% were similar at both temperatures and were better than those over the catalysts with higher loading amounts. The unsupported $FePO_4$ showed the poorest rate of oxygenate formation based on the amount (per gram) of $FePO_4$. We speculate that the larger rate of oxygenate formation over the sample with lower loading amount results from the higher dispersion of $FePO_4$ species inside the mesopores of MCM-41.

Fig. 8 shows the selectivity to oxygenates as a function of CH_4 conversion at 300–500 °C with N_2O. It can be seen that, as compared with the unsupported $FePO_4$, the supported catalysts with loading amounts of 20 and 40 wt% could exhibit higher selectivity to oxygenates at the same CH_4 conversion level and such a tendency could be sustained in the whole range of CH_4 conversion investigated over the catalyst with a loading amount of 40 wt%. Selectivity to oxygenates of

Table 4
MCM-41-supported iron phosphate catalysts for partial oxidation of methane using nitrous oxide

Catalyst	T (°C)	N_2O conversion (%)	CH_4 conversion (%)	Selectivity (%)				Oxyg. yield (%)	Rate of oxyg. formation (mmol h^{-1} g-$FePO_4^{-1}$)
				CH_3OH	HCHO	CH_3OCH_3	Sum of oxyg.[a]		
MCM-41	400	0.70	0.05	0	78.2	0	78.2	0.04	–
	450	1.30	0.11	0	66.1	0	66.1	0.07	–
9 wt% $FePO_4$/	400	0.80	0.30	15.0	60.9	13.3	89.2	0.27	8.0
MCM-41	450	3.20	1.15	15.1	57.5	11.4	83.9	0.97	28.9
20 wt% $FePO_4$/	400	1.43	0.84	23.6	46.7	25.2	95.4	0.80	10.7
MCM-41	450	6.10	2.38	20.5	47.5	13.4	81.4	1.94	26.0
40 wt% $FePO_4$/	400	1.80	0.98	23.7	48.2	24.7	96.6	0.95	6.4
MCM-41	450	7.10	3.01	17.3	50.7	14.1	82.1	2.47	16.5
60 wt% $FePO_4$/	400	2.50	0.88	20.2	47.4	20.3	87.8	0.77	3.4
MCM-41	450	10.9	3.38	15.8	34.4	7.6	57.7	1.95	8.7
$FePO_4$	400	2.40	0.87	35.3	23.5	34.5	93.4	0.81	0.9
	450	8.10	2.01	32.9	24.9	19.3	77.1	1.55	1.7

Reaction conditions: $P(CH_4) = P(N_2O) = 33.8$ kPa; catalyst, 0.2 g for supported catalysts and 0.5 g for $FePO_4$; total flow rate, 60 ml min^{-1}.
[a] Oxyg. denotes oxygenates.

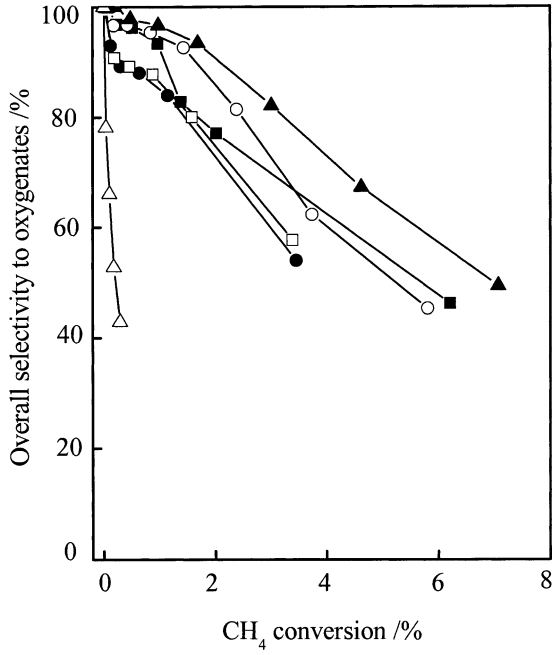

Fig. 8. Overall selectivity to oxygenates versus CH_4 conversion with N_2O. (△) MCM-41, (●) 9 wt% $FePO_4$/MCM-41, (○) 20 wt% $FePO_4$/MCM-41, (▲) 40 wt% $FePO_4$/MCM-41, (□) 60 wt% $FePO_4$/MCM-41, (■) $FePO_4$. Conditions: $W = 0.20$ g (for supported catalysts) and 0.50 g (for $FePO_4$), $F = 60$ ml/min, $P(CH_4) = 33.8$ kPa, $P(N_2O) = 33.8$ kPa, $T = 300$–500 °C.

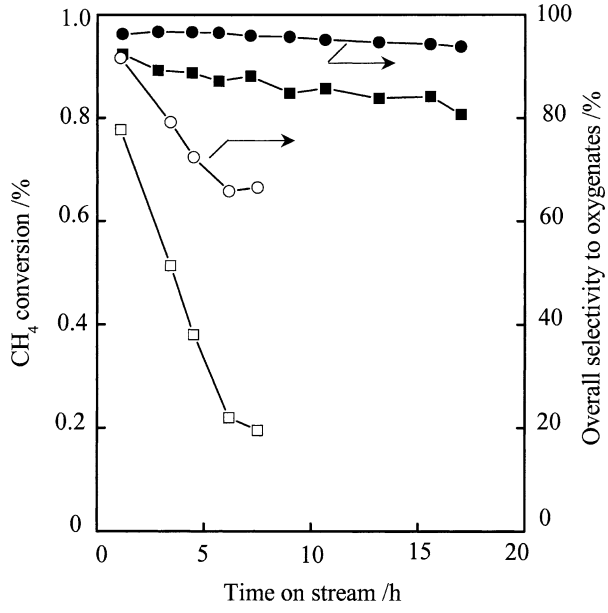

Fig. 9. CH_4 conversion and overall selectivity to oxygenates versus time on stream with N_2O over $FePO_4$ and the 40 wt% $FePO_4$/MCM-41. A 40 wt% $FePO_4$/MCM-41: (■) CH_4 conversion, (●) overall selectivity to oxygenates. $FePO_4$: (□) CH_4 conversion, (○) overall selectivity to oxygenates. Conditions: $W = 0.20$ g (40 wt% $FePO_4$/MCM-41) and 0.25 g ($FePO_4$), $F = 60$ ml/min, $T = 400$ °C, $P(CH_4) = 33.8$ kPa, $P(N_2O) = 33.8$ kPa.

ca. 50% remained at a CH_4 conversion of ca. 7% over this catalyst at 500 °C, and the space time yield of the oxygenates was 9.5 mol h^{-1} kg_{cat}^{-1} under the same conditions.

3.4. Stability of catalytic performances

Both the supported and the unsupported catalysts were stable during the partial oxidation of CH_4 with O_2. No significant changes in CH_4 conversion and HCHO selectivity were observed under the reaction conditions used in Table 3 or Fig. 7. However, when N_2O was used as the oxidant, the catalytic performance dropped with increasing time on stream. Fig. 9 shows that, over $FePO_4$, CH_4 conversion decreases gradually from 0.78 to 0.20%, and the selectivity to oxygenates decreases from 92 to 66% after 7.5 h of reaction under the conditions shown in the figure. The color of the catalyst was changed from yellowish white to black after the reaction, strongly indicating the occurrence of carbon

deposition. On the other hand, the catalytic performances were not significantly decreased with increasing time on stream over the $FePO_4$/MCM-41; CH_4 conversion changed from 0.92 to 0.81% and the selectivity to oxygenates varied from 96 to 94% after 17 h of reaction over the 40 wt% $FePO_4$/MCM-41 under similar reaction conditions. No carbon deposition was observed over this supported catalyst after reaction.

3.5. Kinetic features over the supported iron phosphate catalyst

3.5.1. Partial oxidation of CH_4 with O_2

In the previous paper [8], it has been clarified that HCHO was the primary product and the consecutive oxidation of HCHO gave carbon oxides (CO_x) during the oxidation of CH_4 with O_2 over $FePO_4$. Investigations of the effect of the contact time on the product distributions for the oxidation of CH_4 with O_2 over the 40 wt% $FePO_4$/MCM-41 provided the same conclusion.

Further kinetic studies with this supported catalyst revealed that the rate of CH_4 conversion was almost unchanged with changing O_2 partial pressure from 5 to 70 kPa at a constant CH_4 partial pressure (33.8 kPa), but increased proportionally to CH_4 partial pressure (0–84 kPa) at a constant O_2 partial pressure (16.9 kPa). Therefore, the rate of CH_4 conversion could be expressed with Eq. (1) in the pressure ranges investigated in this study, where k is the rate constant,

$$r(CH_4) = kP(CH_4). \quad (1)$$

The results described here are similar to those obtained for $FePO_4$ reported previously [8]. Such a kinetic equation strongly suggests a redox mechanism, i.e., CH_4 is activated and converted by the lattice oxygen of the surface, and the partially reduced surface is recovered by O_2 in the next step. The replenishment of the surface oxygen by O_2 proceeds very rapidly, and thus the rate is controlled by the activation and the conversion of CH_4 with the oxygen species.

3.5.2. Partial oxidation of CH_4 with N_2O

Fig. 10 shows the product distribution as a function of the contact time for the oxidation of CH_4 with N_2O over the 40 wt% $FePO_4$/MCM-41 at 375 °C. The decrease in the contact time from 0.4 to 0.1 s g ml^{-1} did not significantly change the selectivities to CH_3OH, HCHO, and CH_3OCH_3. A further decrease in the contact time to 0.05 s g ml^{-1} only slightly increased the selectivity to CH_3OH and decreased that to HCHO, and the change for CH_3OCH_3 was unnoticeable. It is generally regarded that HCHO and CH_3OCH_3 could be formed from the oxidation and the dehydration of CH_3OH, respectively. However, the result shown in Fig. 10 tends to suggest that these oxygenates may be formed in parallel from the intermediates such as CH_3 and CH_3O species adsorbed on the surface.

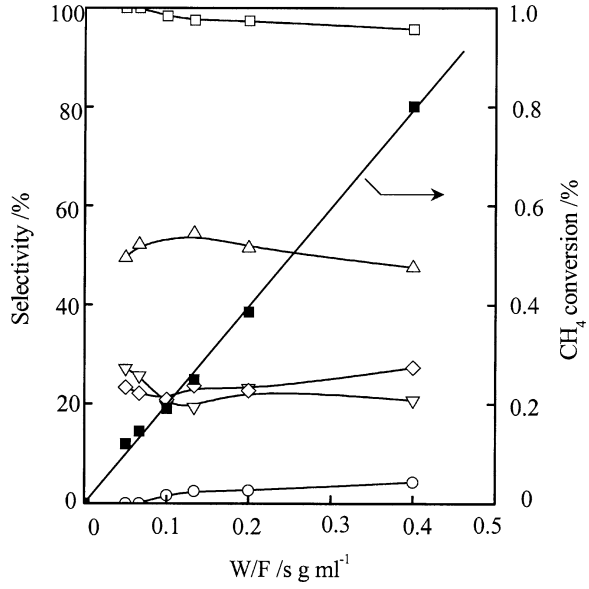

Fig. 10. CH_4 conversion and product selectivities for CH_4 oxidation with N_2O as a function of W/F over the 40 wt% $FePO_4$/MCM-41 catalyst. (■) CH_4 conversion, (▽) CH_3OH selectivity, (△) HCHO selectivity, (◇) CH_3OCH_3 selectivity, (□) total oxygenates selectivity, (○) CO_x selectivity. Conditions: $W = 0.20$ g, $T = 375$ °C, $P(CH_4) = 33.8$ kPa, $P(N_2O) = 33.8$ kPa.

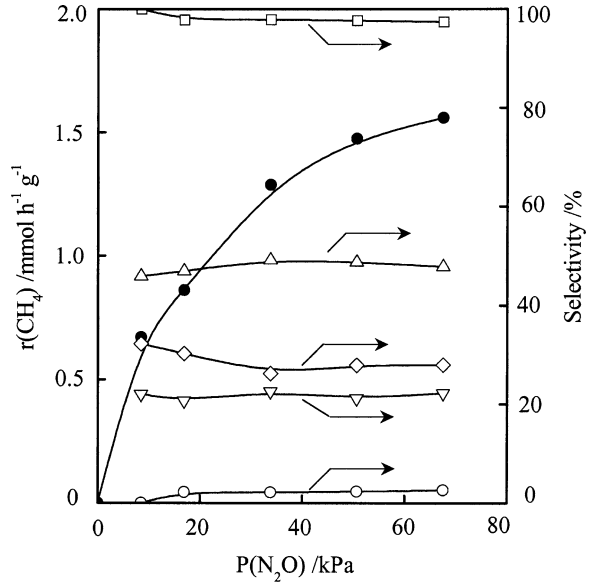

Fig. 11. Effect of the partial pressure of N_2O on CH_4 conversion rate and product selectivities over the 40 wt% $FePO_4$/MCM-41 catalyst. (●) CH_4 conversion rate, (▽) CH_3OH selectivity, (△) HCHO selectivity, (◇) CH_3OCH_3 selectivity, (□) total oxygenates selectivity, (○) CO_x selectivity. Conditions: $W = 0.20$ g, $T = 375$ °C, $F = 60$ ml/min, $P(CH_4) = 33.8$ kPa.

Figs. 11 and 12 show the effects of N_2O and CH_4 partial pressures on CH_4 conversion rate and product selectivities over the 40 wt% $FePO_4$/MCM-41 at 375 °C. Different from the results observed in the case of using O_2, the rate of CH_4 conversion depended on the partial pressures of both CH_4 and N_2O with reaction orders between 0 and 1.

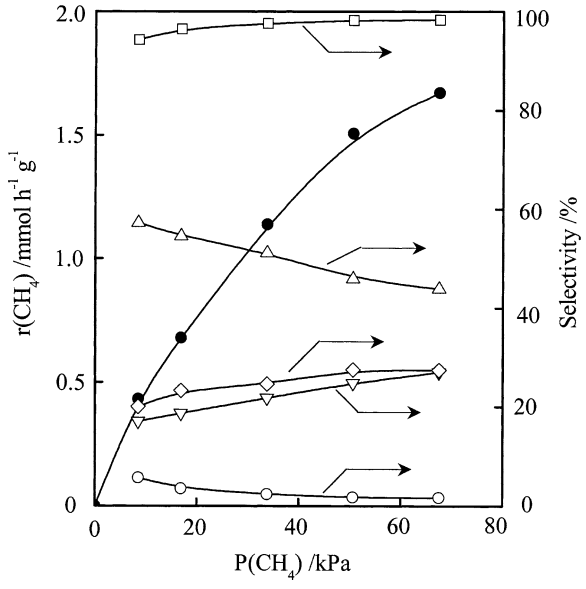

Fig. 12. Effect of the partial pressure of CH_4 on CH_4 conversion rate and product selectivities over the 40 wt% $FePO_4$/MCM-41 catalyst. (●) CH_4 conversion rate, (▽) CH_3OH selectivity, (△) HCHO selectivity, (◇) CH_3OCH_3 selectivity, (□) total oxygenates selectivity, (○) CO_x selectivity. Conditions: $W = 0.20$ g, $T = 375\,^{\circ}C$, $F = 60$ ml/min, $P(N_2O) = 33.8$ kPa.

From Fig. 12, it is seen that the selectivity to HCHO is increased and those to CH_3OH and CH_3OCH_3 are decreased with decreasing the partial pressure of CH_4 at a constant N_2O pressure. In other words, higher $P(N_2O)/P(CH_4)$ leads to higher HCHO selectivity and lower CH_3OH and CH_3OCH_3 selectivities. Slight decreases in the selectivities to CH_3OH and CH_3OCH_3 were also observed as the partial pressure of N_2O was increased at a constant CH_4 pressure in Fig. 11. Simultaneously, the selectivity to HCHO was slightly increased, but such an increase was not noticeable.

These kinetic features allow us to assume that Eqs. (2) and (3) may proceed with comparable rates. In other words, neither the activation of N_2O nor the conversion of CH_4 would proceed overwhelmingly faster than the other:

$$N_2O + Fe^* \rightarrow N_2 + Fe\text{–}O^*(a), \tag{2}$$

$$CH_4 + Fe\text{–}O^*(a) \rightarrow CH_3(a) + OH(a) + Fe^*. \tag{3}$$

The Fe^* and $Fe\text{–}O^*(a)$ in these equations represent the active site and the active oxygen species. By steady-state approximation for the surface concentration of the $Fe\text{–}O^*(a)$, the rate of CH_4 conversion can be deduced as follows:

$$r(CH_4) = k_2 P(CH_4) \frac{N k_1 P(N_2O)}{k_1 P(N_2O) + k_2 P(CH_4)}, \tag{4}$$

where N denotes the total concentration of the active sites, and k_1 and k_2 are the rate constants of Eqs. (2) and (3), respectively.

Eq. (4) has been fitted by plotting $1/r(CH_4)$ versus $1/P(N_2O)$ at a constant pressure of CH_4 and versus $1/P(CH_4)$ at a constant pressure of N_2O, respectively. Good straight lines have been obtained in both plots over either the 40 wt% $FePO_4$/MCM-41 or $FePO_4$, supporting that the assumption described above is reasonable. Further calculations provided us the ratio of k_1/k_2; the values at 375 °C for the 40 wt% $FePO_4$/MCM-41 and $FePO_4$ were 2.0 and 1.0, respectively. This result suggests that the activation of N_2O over the supported catalyst proceeds relatively faster than that over $FePO_4$ if we assume that the same oxygen species accounts for CH_4 conversion in both cases. This probably explains the result that the selectivity to HCHO is remarkably higher over the supported catalysts than that over $FePO_4$ under similar reaction conditions. Moreover, this may also be the reason why carbon deposition occurs over $FePO_4$ but does not take place over the supported catalyst.

3.6. Supporting effects and structure-property relationships

As described above, the characterizations with N_2 adsorption, XRD, and XPS studies tend to suggest that the $FePO_4$ species over the supported catalysts with loading amounts lower than 40 wt% are probably located inside the mesopores of MCM-41, dispersing on the wall surface or forming possibly nano-order small clusters. As loading amount reaches or exceeds 40 wt%, the clusters begin to aggregate outside the mesopores to form small crystalline particles which are mainly composed of the tridymite-like phase of $FePO_4$. On the other hand, the unsupported $FePO_4$ mainly contains a quartz-like phase. It is known that the local structure is the same for the tridymite-like and the quartz-like phases; i.e., iron in both cases is in tetrahedral coordination and the tetrahedrally coordinated iron sites are isolated from each other by phosphate groups [22]. Raman spectroscopic studies suggest that the local structure of iron in the $FePO_4$ species inside the mesopores of MCM-41 also resembles that in the unsupported $FePO_4$.

However, the redox properties of the $FePO_4$ species inside the mesopores are different from those of the tridymite-like and the quartz-like crystalline phases. The supported $FePO_4$ species could be reduced at remarkably lower temperatures as compared with the crystalline phases. This arises probably from the high dispersion of the supported species on the wall surface of MCM-41 or from their small sizes because of the limit of the mesopores. The higher Fe/P ratio (0.80–1.16, approaching the stoichiometric ratio) on the "surface" of the supported $FePO_4$ species as compared with that (0.59) on the surface of the bulk $FePO_4$ may also contribute to changes in their redox properties.

The results from the catalytic reactions show that, with either O_2 or N_2O, the supported samples with loading amounts of 20–40 wt% exhibit both higher activity and higher selectivity to oxygenates than the unsupported $FePO_4$. Furthermore, if the comparison is made on the basis of the amount of $FePO_4$ species (per gram of $FePO_4$), the catalyst with lower loading amount, viz. 9 or 20 wt%, exhibits higher rates of oxygenate formation during the oxidation of CH_4 with N_2O as shown in Table 4. These results strongly suggest that the highly dispersed $FePO_4$ species inside the mesopores of

MCM-41 are more effective in the conversion of CH_4 to useful oxygenates than the bulk $FePO_4$.

The kinetic studies indicate that the conversion of CH_4 to HCHO with O_2 proceeds through a redox mechanism over the supported $FePO_4$, which is similar to that proposed for the unsupported $FePO_4$. The easy reduction at relatively lower temperatures for the supported $FePO_4$ species may enhance the redox process during the conversion of CH_4 to HCHO with O_2, and thus increases the conversion of CH_4 to HCHO.

As for the conversion of CH_4 with N_2O, the analyses of the kinetic data suggest that the activation of N_2O proceeds at a comparable rate with the conversion of CH_4 over the supported $FePO_4$ catalyst. This was also the case for the reactions with N_2O over the unsupported $FePO_4$. However, the activation of N_2O to active oxygen species becomes relatively faster over the supported catalyst. This increases the proportion of HCHO among oxygenates produced over the supported catalyst. More importantly, the carbon deposition is effectively suppressed over the supported catalyst. The enhancing effect for the activation of N_2O due to supporting may also be caused by the ready reduction of the $FePO_4$ species over the supported catalyst because N_2O must be reductively activated by accepting an electron to forming N_2 and active oxygen species such as O^- on Fe^{2+} sites as proposed in the previous study [11].

4. Conclusions

The iron phosphate species are probably located inside the mesopores of MCM-41, forming small clusters or highly dispersing on the wall surface if the loading amount is lower than 40 wt%. Higher loading amount leads to the appearance of crystalline phases containing mainly tridymite-like phase, while the unsupported iron phosphate comprises mainly a quartz-like phase. The iron phosphate species dispersed in the mesopores of MCM-41 could be reduced at remarkably lower temperature as compared with the crystalline iron phosphates. The conversion of methane with nitrous oxide occurs at relatively lower temperatures, and methanol, formaldehyde, and dimethyl ether are formed over both the supported and the unsupported catalysts, while formaldehyde is the only partial oxidation product with oxygen. As compared with the unsupported iron phosphate, the supported catalysts with loading amounts of ca. 20–40 wt% exhibit higher activity and selectivity to oxygenates with either oxidant. The partial oxidation of methane with oxygen proceeds with a redox mechanism, and the replenishment of the surface oxygen by gaseous oxygen takes place rapidly. On the other hand, the activation of nitrous oxide proceeds at a comparable rate with the conversion of methane. The use of supported catalysts instead of iron phosphate noticeably enhances the activation of nitrous oxide, and thus inhibits the carbon deposition and leads to higher stability. The supporting effects for the improvement of iron phosphate in the partial oxidation of methane are proposed to relate with the improved redox properties.

Acknowledgments

This work was supported by the National Natural Science Foundation of China (Nos. 20273054 and 20021002), the Chinese Ministry of Science and Technology (No. G1999022408), the Scientific Research Foundation for the Returned Overseas Chinese Scholars, State Education Ministry, and the Creative Research Foundation for Young Scientists by Fujian Province of China (No. 2001J029).

References

[1] R. Pitchai, K. Klier, Catal. Rev. Sci. Eng. 28 (1986) 13.
[2] M.J. Brown, N.D. Parkyns, Catal. Today 8 (1991) 305.
[3] O.V. Krylov, Catal. Today 18 (1993) 209.
[4] N.D. Parkyns, C.I. Warburton, J.D. Wilson, Catal. Today 18 (1993) 385.
[5] T.J. Hall, J.S.J. Hargreaves, G.J. Hutchings, R.W. Joyner, S.H. Taylor, Fuel Proc. Technol. 42 (1995) 151.
[6] K. Otsuka, Y. Wang, Appl. Catal. A 222 (2001) 145.
[7] K. Tabata, Y. Teng, T. Takemoto, E. Suzuki, M.A. Banares, M.A. Pena, J.L.G. Fierro, Catal. Rev. Sci. Eng. 44 (2002) 1.
[8] Y. Wang, K. Otsuka, J. Catal. 155 (1995) 256.
[9] Y. Wang, K. Otsuka, Chem. Lett. (1994) 1893.
[10] Y. Wang, K. Otsuka, J. Chem. Soc. Faraday Trans. 91 (1995) 3953.
[11] Y. Wang, K. Otsuka, J. Catal. 171 (1997) 106.
[12] Y. Wang, K. Otsuka, J. Mol. Catal. A 111 (1996) 341.
[13] T. Kobayashi, N. Guilhaume, J. Miki, N. Kitamura, M. Haruta, Catal. Today 32 (1996) 171.
[14] A. Parmaliana, F. Arena, F. Frusteri, A. Martínez-Arias, M. López Granados, J.L.G. Fierro, Appl. Catal. A 226 (2002) 163.
[15] G.O. Alptekin, A.M. Herring, D.L. Williamson, T.R. Ohno, R.L. McCormick, J. Catal. 181 (1999) 104.
[16] R.L. McCormick, G.O. Alptekin, D.L. Williamson, T.R. Ohno, Top. Catal. 10 (2000) 115.
[17] S. Lim, G.L. Haller, Appl. Catal. A 188 (1999) 277.
[18] H. Berndt, A. Martin, A. Bruckner, A. Schreier, E. Muller, D. Kosslick, G.-U. Wolf, B. Lucke, J. Catal. 191 (2000) 384.
[19] Q. Zhang, Y. Wang, Y. Ohishi, T. Shishido, K. Takehira, J. Catal. 202 (2001) 308.
[20] M.L. Pena, A. Dojoz, V. Fornes, F. Rey, M.I. Vazquez, J.M. Lopez Nieto, Appl. Catal. A 209 (2001) 155.
[21] Y. Wang, Q. Zhang, T. Shishido, K. Takehira, J. Catal. 209 (2002) 186.
[22] A.M. Beale, G. Sankar, J. Mater. Chem. 12 (2002) 3064.
[23] P. Bonnet, J.M.M. Millet, C. Leclercq, J.C. Védrine, J. Catal. 158 (1996) 128.